Article

Silver Nanocatalyst Supported on Waste-Based Polystyrene Foam for Thermal and Plasmonic Reduction of *p*-Nitrophenol

Welida T. A. da Silva,[a] Geovânia C. de Assis,[ ]*,[b] Roberta A. de Jesus,[ ][c]
Rayssa J. B. Motta,[ ][d] Luiz Fernando R. Ferreira,[c] Yolice Patricia M. Ruiz,[e]
André Galembeck,[e] Ricardo Schneider[f] and Rodrigo J. de Oliveira[ ]*,[a]

[a]*Laboratório de Físico-Química de Materiais (PCMLab), Departamento de Química,*
Universidade Estadual da Paraíba, 58429-500 Campina Grande-PB, Brazil

[b]*Grupo de Pesquisa em Processos Oxidativos Avançados (AdOx), Departamento de Engenharia Química,*
Escola Politécnica, Universidade de São Paulo, 05508-010 São Paulo-SP, Brazil

[c]*Instituto de Tecnologia e Pesquisa, Universidade Tiradentes, 49032-490 Aracaju-SE, Brazil*

[d]*Grupo de Catálise e Reatividade Química, Instituto de Química e Biotecnologia,*
Universidade Federal de Alagoas, 57072-970 Maceió-AL, Brazil

[e]*Laboratório de Compostos Híbridos, Interfaces e Colóides (CHICO), Departamento de Química Fundamental,*
Universidade Federal de Pernambuco, 50740-560 Recife- PE, Brazil

[f]*Grupo de Polímeros e Nanoestruturas, Universidade Tecnológica Federal do Paraná (UTFPR),*
85902-490 Toledo-PR, Brazil

Disposal of plastics into the environment has been one of the major problems for the environment. The accumulation of polystyrene (PS) occurs in an accelerated way and, therefore, its reuse is challenging. Polystyrene nanocomposites impregnated with Ag nanoparticles (PS/AgNP) are generated from polystyrene residues and can be applied in the catalytic and plasmonic photo-catalytic reduction of phenolic compounds such as *p*-nitrophenol (PNP) to *p*-aminophenol (PAP). The AgNP were synthesized by a reverse micelle method resulting in nanoparticles with sizes in a range of 31.1-34.0 nm. The organocolloid was characterized by UV-Vis and dynamic light scattering (DLS), demonstrating the preparation of spherical nanoparticles. The preparation of the PS/AgNP, obtained using a thermally induced phase separation method (TIPS), was confirmed by means of scanning electron microscopy (SEM), X-ray diffraction (XRD), laser-induced breakdown spectroscopy (LIBS), and Fourier transform visible infrared spectroscopy (FTIR). Nanocomposites showed impressive performance in the catalytic and plasmonic photocatalytic reduction under blue light irradiation, reaching up to 98% conversion, being a promising material for wastewater treatment as well as other various environmental issues. We used blue light to observe the plasmonic effect of silver nanoparticles, and no previous reports of this composite for PNP reduction using blue light photocatalysis were found.

Keywords: environmental remediation, plasmonic catalysis, polymer waste, nanoparticles

Introduction

Pollution of water bodies is caused by various persistent and dangerous non-biodegradable substances,[1,2] including organic compounds such as pesticides,[3] pharmaceuticals,[4] personal care products,[5] dyes,[6] phenolic compounds,[7] and microplastics,[2] among others. These substances cause serious problems for the environment and human health, as demonstrated in previous investigations,[1,2] and, therefore, their removal has been a topic of research by the scientific community in order to try to minimize their impacts. Among the substances mentioned above, phenolic compounds are produced by a wide variety of industries, such as the petrochemical,[8] textile,[9] food processing,[10] pesticides,[11]

among others and, thus, they are often released into the environment during production and use.[12] As a result, a huge volume of contaminated effluents is discharged into the environment without prior treatment.

Among the nitroaromatic compounds, *p*-nitrophenol (PNP) is one of the main emerging organic pollutants.[9] It is known that nitrophenols are very important starting materials for the production of aminophenols and other chemicals,[13] but nitrophenols are toxic and therefore dangerous in the environment. The catalytic reduction of PNP results in the formation of *p*-aminophenol, a compound with a lower toxicity than PNP, which is considered a valuable input in the pharmaceutical industries as it is used for the production of aniline, paracetamol, phenacetin and acetanilide,[13] in addition to being applied as a corrosion inhibitor, photographic developer and as a reagent for the synthesis of many dyes.[14] This reaction with high environmental and pharmaceutical interest was first reported by Pradhan *et al.*[15] in the presence of Ag and BH_4^- nanoparticles.[15] Usually, the methods used for the reduction of *p*-nitrophenol involve iron and tin acids as reducing agents.[14]

Due to their chemical structure, phenolic compounds are difficult to biodegrade and have a bioaccumulate tendency.[12] These compounds can enter the food chain through wastewater contamination, threatening human health and representing a serious environmental problem.[16] PNP, in particular, is a dangerous type of phenolic compound that has been the focus of investigations.[16]

The presence of PNP and its analogues in the environment has become a major concern in recent years, as their presence in receiving water bodies can cause serious environmental and public health problems, such as damage to the kidneys, liver and central nervous system of living creatures, and must be treated before being discarded into the environment.[11] There are already several technologies used for PNP removal and degradation, such as photocatalytic oxidation,[17] adsorption,[9] catalytic degradation,[16] and catalytic reduction.[18] Among these technologies, catalytic reduction is of particular interest due to its high efficiency, simple operation, and relative low maintenance cost.[18,19] Thus, the PNP reduction to *p*-aminophenol (PAP), using sodium borohydride ($NaBH_4$) as a reducing agent in the presence of a catalyst, has received considerable attention in the scientific literature,[20,21] particularly in the search for more efficient technologies for the removal and degradation of these dangerous compounds.

Several metallic nanoparticles, including noble metals, such as Au,[22] Ag,[23] are commonly used in this type of process due to the surface plasmonic resonance effect that enables the excitation of electrons in the conduction band, causing an oscillation able to result in a resonance and production of radicals, such as the hydroxyl radical (•OH), in addition to creating active sites capable of causing catalytic reduction of compounds.[24]

Metallic nanoparticles, such as silver, are used to remedy many situations, such as pollution by organic dyes, reducing them, among which Methylene Blue[25] and PNP.[26] In addition, it is used in the degradation of cyanotoxins, such as shown by Benamara *et al.*,[27] and in applications in the medical field acting as an antimicrobial agent.[28] dos Santos Jr. *et al.*[29] used silver nanoparticles (AgNP) stabilized with chitosan biopolymer with sizes of 8.7 ± 3.1 nm for caries treatment. Some of the samples presented small percentages of triangular nanoparticles and were efficient against *Streptococcus mutans* and were considered equivalent to chlorhexidine, the standard antibiotic in dentistry.[29]

Plasmonic photoinduced resonance is also becoming a powerful tool in nanocatalysis.[30] Since the first investigations of nanoparticles with resonance effect,[31] numerous reactions have been carried out on Ag and Au surfaces, showing that the irradiation of low intensity visible photons significantly increases the rate of chemical reactions.[23,32]

The light plays an important role in the excitation of electrons, whether inside the metallic catalyst by the plasmonic effect and/or by the excitation of the band. These phenomena open alternative reaction pathways that are not so easily accessed only through the input of thermal energy.[33] The plasmonic excitation of these nanoparticles, caused by an external electric field, causes charge dampening where electrons move generating peaks.[34,35] These peaks, when interacting with light, create places of higher energy density, which allow photocatalytic processes under lower radiation intensity which also make them very efficient.[34,35] Chen *et al.*[36] reported the use of AgNP to degrade phenol and drive the oxidation of benzyl alcohol to benzaldehyde under ultraviolet light. This points to the role of the localized surface plasmon resonance (LSPR) effect and the transition between AgNP bands in the activation of organic molecules for oxidation under UV-Vis irradiation.[36]

Catalytic nanoparticles, such as AgNP, are often unstable and can irreversibly aggregate during catalytic reactions due to their high surface energies; in addition, high costs are associated with their recovery and subsequent reuse.[37,38] Such issue may be sorted out by entrapment of the nanoparticle on substrates, enabling a dispersion of the metal on the surface of the support, beneficially influencing the catalytic activity.[39,40] Many types of catalyst support with different morphologies have been employed, including carbon,[41] silica materials,[42] polymeric materials[43]

among others. Polymeric materials have received increasing attention due to their high strength, recyclability, accessibility of catalytic sites and efficient catalytic activity when used to support a catalyst.[6,44]

Polymers waste can be recycled to produce new materials with desired properties. Plastic waste is considered a technically viable material for use as a catalytic support, and the literature has shown that supported catalysts are in high demand because their mesoporous structure expose active metallic centers, favoring a homogeneous distribution of active sites on the surface and consequently improving the performance of catalytic action to destroy and/or produce desirable products.[6,39,45] The nanocatalyst-support interactions in these materials can have a substantial influence on catalysis, making the modulation of this interaction one of the few tools capable of improving catalytic performance.[46] Polystyrene (PS), as one of the top five most consumed plastics, has been widely applied in electronics, construction, transportation, packaging and other daily supply industries.[47] Due to its wide ranges of production and use, a large amount of PS waste is dumped into the environment every year, especially into the marine environment, severely threatening the global biosphere.[47] However, research has shown satisfactory results in the destination of PS waste for various applications, for example, PS waste has been applied as catalytic supports, with satisfactory results.[6,48-50]

Aubert and Clough[51] showed in 1985 a procedure in which low density micro and macrostructured polymeric foams were synthesized from PS solutions in cyclohexane/benzene solvent, taking advantage of temperature induced phase separation. Steytler and Robinson[52] demonstrated that freezing water-in-oil microemulsion leads to increased attractive interactions among dispersed phase; the same happens for calcium carbonate nanoparticles in cyclohexane, which lead to the formation of inorganic foams.[52] As an example, the synthesis of PS nanocomposite incorporated with nanoparticles is carried out using the thermally induced phase separation (TIPS) method,[53] which allows the rapid formation of porous and nanoparticle surface decorated catalytic polymeric foams.[6] This method not only allows adjustment of particle size, porosity and pore morphology, but it can also allow the inclusion of active ingredients such as small molecules or nanoparticles in the polymer matrix.[6,53]

The synthesis of polymeric nanocomposite doped with other materials such as TiO_2 or nanoparticles has been extensively studied.[54-56] Our research group described the use of PS residues in nanocomposite synthesis as support for nanostructured SnO_2 and its application in the photodegradation of rhodamine B.[6] It was observed that

the support influenced the increase in surface area and promoted greater efficiency in the photodegradation of the dye.[6] Nanocomposites can be alternative supports to be used for catalytic applications, since they present high resistance and their porosity is easily modified, which results in good dispersion of nanoparticles on its surface. Rolison[57] says that "New opportunities for improved performance" comes from the "use of nothing (void space) and deliberate disorder as design components", and this resonates with polymeric nanocomposites structures.

Despite the enormous research work already carried out to develop new composites for environmental decontamination, a search for new materials capable of converting polystyrene waste on support for catalytic nanoparticles to destroy organic contaminants is still extremely relevant. In particular, catalytic reduction and plasmonic photocatalysis in the presence of silver nanoparticles are interesting alternatives for this purpose. The preparation of polymeric composites based on polystyrene residues to support plasmonic nanoparticles, associated with the adsorption capacity of the organic dye on its surface, can increase the photocatalytic activity of the material. Here, we approach two environmental issues, the recycling of PS waste, turning it into PS/AgNP based catalytic nanocomposites through the TIPS method, and the application of this composite for PNP reduction under thermocatalytic and plasmonic photocatalytic ways. It is important to highlight that in the present study we used blue light to observe the plasmonic effect of silver nanoparticles, and no previous reports of this composite for PNP reduction using blue light photocatalysis were found.

Experimental

Synthesis of AgNP

AgNP were synthesized using the microemulsion method.[58,59] This process involves the preparation of two microemulsions, A and B, incorporating the different reagents. Here, the influence of some parameters to obtain AgNP was investigated, such as sodium borohydride ($NaBH_4$, Neon/99.0%, Suzano, São Paulo, Brazil) concentration (0.382 and 3.82 mol L^{-1}), hexadecyltrimethylammonium bromide (CTAB, $C_{19}H_{42}NBr$, Neon/98.0%, Suzano, São Paulo, Brazil) concentration 0.004 to 0.270 mol L^{-1}, silver nitrate ($AgNO_3$, Neon/99.8%, Suzano, São Paulo, Brazil) concentration 0.0382 and 0.00764 mol L^{-1}, and purification time (30 and 1440 min). Initially, the concentration of $NaBH_4$ was evaluated. For this, aqueous solutions of $AgNO_3$ (0.0382 mol L^{-1}), cyclohexane (C_6H_{12}, Neon/98.0%, Suzano, São Paulo, Brazil))/1-propanol

(C_3H_8O, Vetec/95.0%, Duque de Caxias, Rio de Janeiro, Brazil) mixture as solvent (4:1 in volume) and $NaBH_4$ (0.382 and 3.82 mol L^{-1}) were prepared, and CTAB was used as NPs stabilizer/micelles structure. To assess the influence of the $NaBH_4$ concentration, two microemulsions (microemulsion A and microemulsion B) were prepared; for each of them, CTAB was dissolved in 3.5 mL of the cyclohexane/1-propanol solution. After complete dissolution of the CTAB, 81 µL of $NaBH_4$ solution (0.382 mol L^{-1}) in microemulsion A and 81 µL of $AgNO_3$ solution (0.0382 mol L^{-1}) in microemulsion B were added under stirring until formation of a stable microemulsion. Subsequently, microemulsion B was added directly to microemulsion A, and kept under constant stirring for 30 min, after which 1.4 mL of deionized water was added and hand's shacked for 5 min, thus promoting phase separation after resting. The supernatant, containing AgNP organocolloid, was collected after 1440 min. This procedure was performed for $NaBH_4$ (0.382 mol L^{-1}) and later for $NaBH_4$ (3.820 mol L^{-1}). It is important to highlight that the CTAB was recovered in the purification process of NP in the aqueous phase.

Synthesis of AgNP impregnated polystyrene nanocomposites (PS/AgNP)

The PS/AgNP nanocomposites were obtained by a TIPS method, as described in the literature.[6] In the synthesis of nanocomposites, it was used PS for decoration obtained in the dense pellet form from a local market from Campina Grande, Paraíba, Brazil, and used as received. The PS concentration in the cyclohexane precursor mixture ranged between 5 and 7% (m/v). PS was solubilized into the AgNP organocolloid in weight mass needed to obtain the final weight/volume percentage desired. After the addition of PS, the solutions were kept under stirring and temperature above 36 °C (theta temperature) until the complete dissolution of the PS.[51] To induce phase separation, the colloidal dispersions were frozen using a Peltier system, operating at −10 °C. After 5 min of cooling, a vacuum pump was coupled to the system to remove the cyclohexane by freeze-drying. Nanocomposites formation was observed and confirmed after 30 min of freeze-drying. The low-pressure freeze-drying led to cyclohexane removal by sublimation in the sample leaving behind a solid nanocomposite with a hard "skeleton". The samples were labeled as PS(X)/AgNP(Y), where X is the weight/volume concentration (g mL^{-1} × 100) of PS in cyclohexane (5 or 7%) and Y is the Ag nanoparticles wt.% in the PS nanocomposites. PS(X)/AgNP(Y) were synthesized varying the concentration of Ag (0.2 and 0.4%), the samples

being labeled PS(X)/AgNP(0.2) and PS(X)/AgNP(0.4). To prepare the PS foam, cyclohexane solvent was used instead of organocolloid, being named PS(X).

Characterization

The AgNP size of the organocolloid was estimated using spectroscopy in the UV-Vis region (Shimadzu, model UV-1800, Kyoto, Japan) and dynamic light scattering (DLS) (NanoBrook Omni Particle Analyzer-Brookhaven Instruments, Instrutécnica Ltda, Campinas, Brazil), equipped with a red laser diode (35 mV, λ = 640 nm) and a detector at a 90°. The morphology and diameter of the particles were determined using a scanning electron microscope (SEM, JEOL JSM-IT200LA, Tokyo, Japan), operated with an accelerating voltage of 15 kV. A small section of the foam was sprayed with a thin layer of gold before SEM analysis. To determine the average diameter of the particles, about 190 counts were performed using the ImageJ software.[60] X-ray (XRD) patterns were obtained with the aid of a diffractometer (model SmartLabSE, Rigaku, Tokyo, Japan), using Kα line of Cu (1.540593 Å), voltage 40 kV and current of 30 mA. Scans were carried out at intervals of 2θ between 30 and 80°, with a step of 1.0° *per* min.

The laser-induced breakdown spectroscopy (LIBS) measurements were performed using a J200 Tandem LIBS spectrometer from Applied Spectra, INC, (West Sacramento, California, USA), operating with a 266 nm laser (25 mJ ns and pulse width (FWHM) < 6 ns) and equipped with a 6 channel charge-coupled device (CCD) spectrometer with spectral coverage from 190-1040 nm and resolution better than < 0.1 nm. The measurements were performed using a laser power operating at 5%; the gate delay of 1.0 µs, 10 shots; and the spot size of 50 µm. The spectra obtained were analyzed in relation to the National Institute of Standards and Technology (NIST) database.[61] All experiments were performed under an air atmosphere.

Evaluation of catalytic activity

The catalytic activity of PS(5)/Ag(0.2) and PS(7)/Ag(0.2) nanocomposites in the PNP reduction reaction was evaluated in an open system (beaker) under constant magnetic stirring. The foams were inserted into the aqueous solution with the help of an inert plastic mesh according to Figure S1, Supplementary Information (SI) section. Herein, the influence of some parameters, such as the molar ratio PNP:$NaBH_4$ (1:1000, 1:1320 and 1:6600), concentration of Ag present in the nanocomposites (0.2 and 0.4 %), effect of the PS precursor solution concentration (5 and 7%), and the influence of the presence of blue light in the system

were investigated in terms of their catalytic efficiency. For the photocatalytic tests, a commercial light emitting diode (LED) lamp from OUROLUX, 6 W of power, was used with a flux of 400 lm and emitting wavelength in the blue region between 400-500 nm. The system was placed in a closed photocatalytic reactor measuring 54.5 cm in height, 29.5 cm in width and 54.5 in depth, with a distance from the lamp to the reactor of 20 cm. Assays were performed in triplicate and samples were stored in test tubes covered with aluminium foil to prevent light exposure, prior to spectrophotometric analysis in the UV-Vis region (Shimadzu, model UV-1800, Kyoto, Japan). The tests were carried out following the decrease of the peak at 400 nm, characteristic of *p*-nitrophenolate ion; for this, 100 μL aliquots of the reaction medium were removed over time. The small volume withdrawn does not significantly change the PNP:Ag ratio in the 25 mL total volume system.

Results and Discussion

PS foams

SEM images of PS foams, PS(5) and PS(7) (Figures 1a and 1b, respectively), clearly show that the foam structure was different when varying the polystyrene concentration to obtain it. The foam PS(5) presented aggregated particles, with almost spherical morphology and narrow particle size distribution, with average size of 901 ± 232 nm, forming a semi-rigid structure, of low mechanical resistance when compared to the foam PS(7), which was also composed of aggregated particles, but showed a wider size distribution, indicating that the particles that make up the foam structure are of different sizes, whose average size was 1808 ± 609 nm. The morphology of pure foam PS(7) ranges from spheres with well-defined contours to wider, dense structures, forming thick "walls", due to coalescence of spheres.

The process of obtaining these foams makes use of the phenomenon of phase separation induced by temperature.[6] Aubert and Cough[51] demonstrated that the polymeric chains of PS in cyclohexane, having a theta temperature of approximately 36 °C, behave as ideal chains, without preferential interactions with the solvent or between the chain segments, behaving similarly to the melting state.[51] Below this temperature, there is a phase separation where one of them is rich in PS and the other is poor. With the freezing of the solvent, nuclei rich in PS are formed and trapped in the medium immediately after its formation, giving rise to the particles observed in the SEM images (Figures 1a and 1b). These particles are related to PS formed in the nucleation process that aggregated but did not coalesce to contribute to the skeleton formation. In the
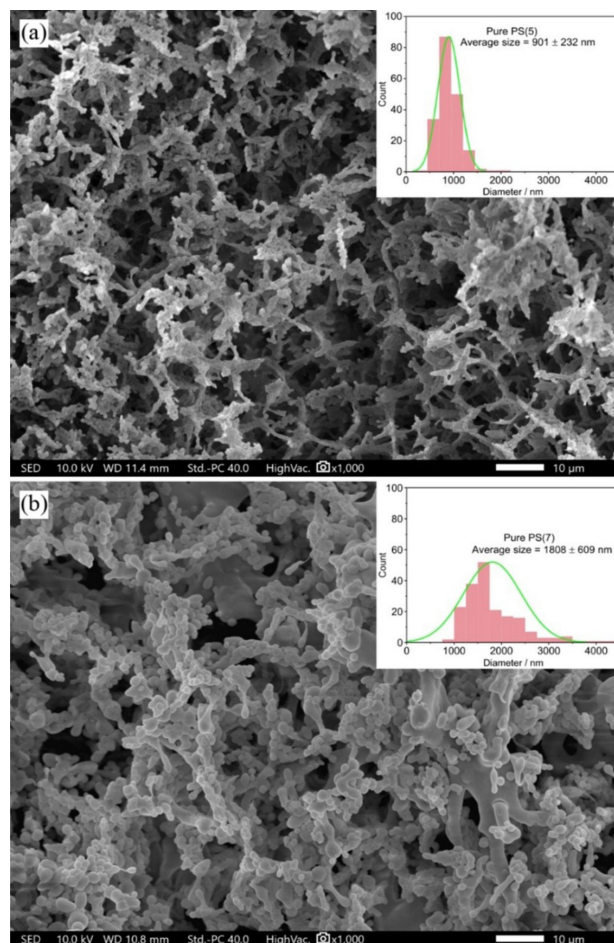
Figure 1. SEM images of the foams (a) PS(5), and (b) PS(7). The inset displays their particle size distribution histograms.

lyophilization process, cyclohexane acted as a porogenic,[62] since with the removal of the solvent, the aggregation of PS nuclei occurred, resulting in a porous material. The final state of the system is a PS foam without the presence of cyclohexane (Figure 1). In relation to porosity, it was a function of the PS concentration in the precursor solution.[51] A lower concentration of PS formed smaller particles, allowing the formation of a more branched, fragile skeleton, as observed in foam PS(5). While a higher concentration of PS allowed the formation of a more robust skeleton due to the greater volume of seeds formed during phase separation. De Assis *et al.*[6] reported that polymer concentration can affect catalytic performance.

AgNP and PS/AgNP nanocomposites

AgNP

The microemulsion method is commonly used to make organocolloids with narrow control of size and polydispersity.[58] In order to make PS foams doped with AgNP, it was useful to prepare firstly the AgNP

organocolloid in the same solvent used for the foam preparation, cyclohexane. For that, the method developed by Hollamby *et al.*[58] was adapted, using cyclohexane instead of octane as solvent.

Figure 2a shows the UV-Vis absorption spectra of the AgNP organocolloid obtained with different concentrations of $NaBH_4$ (0.382 and 3.820 mol L^{-1}). The absorption intensity increases with $NaBH_4$ concentration, i.e., a higher concentration of $NaBH_4$ leads to more and smaller nanoparticles which results in an increase in absorption, corroborating to what was presented by Mulfinger *et al.*[63] and Wang *et al.*[64] who highlighted that this is a result of borohydride adsorption, allowing an increase in particle surface charges, arising from quantities of the reducing agent sufficient to stabilize them as the reaction proceeds. Furthermore, the maximum absorption wavelengths observed at 407 and 411 nm (Figure 2) suggests that the formed particles have only one absorption band showing spherical morphology.[58,65] The theory of Mie[66] is based on a similar discussion that relates the position of the surface plasmon resonance (SPR) band to the morphology of metallic nanostructures that appear spherical for single bands.[66] Hollamby *et al.*[58] obtained similar results in a synthesis of AgNP and AuNP via microemulsion method.

Another indicator of AgNP formation is the visual appearance of the resulting solution (Figure 2b). This yellowish coloration is characteristic of colloidal Ag, observed after the reaction between the silver salt and the reducing agent in solution,[67] being the result of electromagnetic radiation in the visible range, due to SPR band occurring at the time of formation of NPs.[62,63,68]

Narrower bands observed when a higher concentration of $NaBH_4$ was used ($\lambda_{max} = 407$ nm) suggest the formation of smaller particles in the medium (Figure 2b). This formation is the result of a more favored nucleation process in relation to growth,[68] that is, particles of approximately 34 nm are generated according to theoretical simulations using the MiePlot software.[66,69] The narrowing of bands observed can be justified through the values of FWHM, which is directly related to the degree of dispersion of the particles in the medium, and for $\lambda_{max} = 407$ nm, it results in 64.43°. In this case, the formation of particles with less polydispersity predominates and consequently, narrower bands are formed. On the other hand, this feature was not observed using a lower concentration of $NaBH_4$ (0.382 mol L^{-1}), which resulted in $\lambda_{max} = 411$ nm, as a consequence of favoring the growth process, since with less reducing agent a smaller number of nuclei is formed, in addition to having a FWHM equal to 66.05°, resulting in higher polydispersity.

This difference in particle size is also evidenced and confirmed by a blue shift observed in the surface
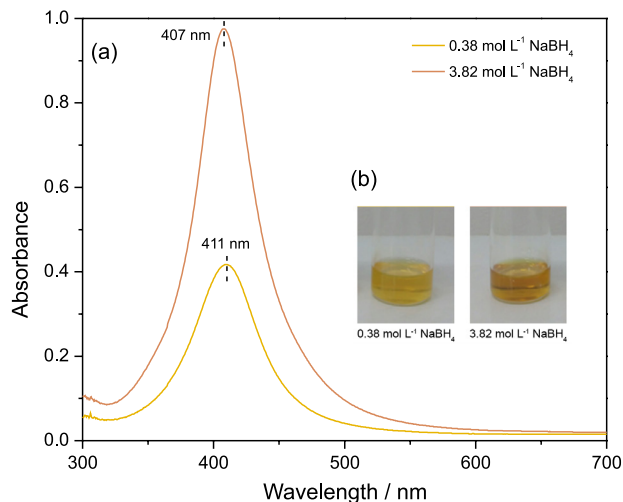
Figure 2. (a) UV-Vis spectra of AgNP at different concentrations of $NaBH_4$, and (b) images of colloidal dispersions at different concentrations of $NaBH_4$, with maximum wavelengths corresponding to the spectral curves.

plasmon band, which is shifted to longer wavelengths (407 → 411 nm).[70] This shift depends on the size and shape of the particle and occurs due to the higher concentration of substrates and/or reagents involved in the reaction. This was also observed by Anandalakshmi *et al.*,[71] when they obtained AgNP using green synthesis, where the deviation is caused by the variation of the leaf extract concentration, while in the present work this deviation is directly associated with the variation of the reducing agent concentration. In this sense, the AgNP synthesized with a concentration of 3.82 mol L^{-1} of $NaBH_4$ was chosen to be worked on because it allows the formation of smaller particles.

UV-Vis absorption curves at different CTAB concentrations from 0.004 to 0.27 mol L^{-1} were studied (Figure S2, SI section). It was observed that the λ_{max} of the AgNP absorption bands at different concentrations of CTAB reflected an increase in particle size as a function of the increase in the concentration of the surfactant (CTAB) (Figure S2b, SI section). CTAB is generally used to block the growth of AgNP being considered one of the main parameters for controlling particle size.[63,71]

Usually, the size of the nanoparticles is proportional to the increase in the concentration of CTAB.[72] The increase in the size of nanoparticles suggests a growth process that occurred in a smaller number of nuclei and proceeded in parallel with nucleation.[72] Husein *et al.*[73,74] showed that a lower amount of Ag^{+} *per* micelle means a lower probability of nucleation since there is a minimum concentration of ions necessary for the formation of nuclei, and, in this case, for nucleation to continue, it becomes dependent on the intermicellar exchange which, by causing an increase in

the number of generated micelles by increasing [CTAB], impairs nucleation and favors particle growth.[72-74] Taking this into account, an increase in particle size caused when the concentration of CTAB increases from 0.004 to 0.27 mol L^{-1} observed by UV-Vis can be compensated by a greater amount of particles existing in the medium, which is seen through the highest intensities of the bands (UV-Vis curves, Figure S2, SI section). This clearly occurs in AgNP samples obtained with 0.27 mol L^{-1} of CTAB, which for this reason was chosen for the study. Observing the optimized conditions of NaBH$_4$ and CTAB concentration, the effect of AgNO$_3$ concentration was also investigated in order to relate parameters, especially size and morphology.

When using a lower concentration of AgNO$_3$ (0.00764 mol L^{-1}) the particle size was 41 nm, while for the highest concentration of AgNO$_3$ (0.0382 mol L^{-1}) it had a size of 31 nm, decreasing considerably with increasing AgNO$_3$ concentration. The size measurement was done by simulation of the UV-Vis spectra using Mie Theory, as discussed below. The decrease in particle size significantly occurs with the higher concentration of AgNO$_3$ and this can be explained once at higher concentrations the nucleation is favored instead of growth, since there is a critical concentration of nucleation,[75] and for smaller Ag$^+$ concentrations, the probability of nuclei formation is lower.

The time spent at the purification step can ensure that the particles are purified without any interference in the medium.[58] The spectra in the UV-Vis region presents the maximum wavelength data which can relate to the particle size, for the purification time of 30 min ($\lambda_{max} = 411$ nm) and for the purification time of 1440 min ($\lambda_{max} = 407$ nm). A theoretical evaluation of SPR bands was performed using the MiePlot software.[69] The model provides a powerful approach to evaluate the scattering of the spherical nanoparticles in different solvents. The model suggests a diameter of 34 nm for 1440 min purified AgNP, while the analysis by DLS provides AgNP with particle sizes of 31.1 nm of diameter (see Figure S3, SI section). It is important to mention that from the theoretical evaluation of the SPR bands using MiePlot, it is only possible to observe the polydispersity analysis up to 20%, which was not enough for these systems. However, for the analysis of the UV-Vis spectra, specific parameters such as, absorbance curve, LSPR peak positions, intensity and FWHM, makes UV-Vis a powerful tool to characterize the evolution of the dispersity of the particles in the medium, as discussed in previous studies.[76] Therefore, in our results presented in Figure S3, we can suggest a trend between FWHM and degree of polydispersity, the greater the FWHM, the greater the polydispersity.[76,77] Also, a slight red-shift of the

LSPR according to the literature[78] is characteristic of an increased size of NPs.

The increase in the purification time decreases the maximum absorption wavelength, being indicative of the occurrence of phase separation, originating an organocolloid phase at the top of the system, as observed by Hollamby *et al.*[58] A lower wavelength suggests smaller particles and is therefore the most ideal to be considered,[79] once particle size is roughly correlated with wavelength absorption due to SPR. It can be expected that lower separation times leads to a mixture of AgNP and water droplets, favoring aggregation and bigger sizes as reflected by the observed maximum SPR wavelengths.

PS/AgNP nanocomposites

In SEM images (Figures 3a and 3b), the nanocomposites PS/AgNP(0.2) showed porous structure, formed by the aggregation/coalescence of PS nuclei/particles. The nanocomposite PS(5)/AgNP(0.2), (Figure 3a), showed a structure composed of thick and wide walls with spherical or nearly spherical particles of varying sizes, with average size of 1508 ± 526 nm. The particles present in this foam were due to the non-coalescence of the PS nuclei, leaving the particles under the surface. The structure of the nanocomposite PS(7)/AgNP(0.2) (Figure 3b) was composed of much smaller, medium-sized particles of 800 ± 299 nm, and thinner walls than those seen in PS(5)/AgNP(0.2). The decrease in particle size in PS(7)/AgNP(0.2) compared to PS(5)/AgNP(0.2) can be attributed to the greater amount of CTAB in relation to the PS present in the nanocomposite PS(5)/AgNP(0.2). Thus, the neutralization of surface charges on the polymeric surface was more efficient in PS(5)/AgNP(0.2), which resulted in a lower repulsion between the particles, helping their coalescence, providing an increase in particle size and densification of the foam skeleton. Furthermore, it was possible to observe that the aggregation of nanocomposite particles in PS(5)/AgNP(0.2) resulted in larger pores than in PS(7)/AgNP(0.2), which can be attributed to the relationship between PS concentration and core sizes. It is worth mentioning that the differences in the pore structure are much more evident for PS/AgNP nanocomposites than for pure foams, a fact that can be associated with the presence of AgNP and CTAB and their effect on PS particle's surface tension.

Generally, systems involving the presence of nanoparticles that use cationic surfactants in their formation, when supported on polymers, can promote the reduction of the amount of negative charges existing on the surface of the polymer, which are the result of
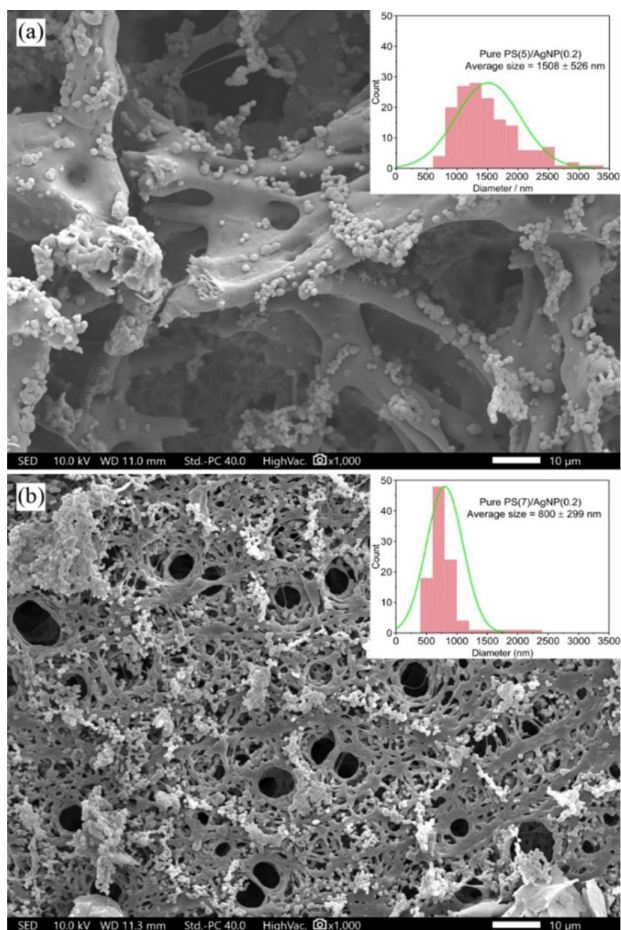
Figure 3. SEM images of the nanocomposites (a) PS(5)/AgNP(0.2), and (b) PS(7)/AgNP(0.2). The inset displays their particle size distribution histograms.

the polymerization process that occurs in the presence of a persulfate oxidizing agent, which in their pure form generate very densified PS foam skeletons.[80] In this sense, the presence of AgNP, and consequently CTAB existing in its dispersion, can partially neutralize these surface charges generated on the polymeric surface, resulting in a decrease in the surface potential and, thus, causing an aggregation of the supported particles, in addition to the densification of the foam skeleton, generating systems with more closed pores, as observed in the SEM (Figure 3b).[80,81]

The Fourier transform infrared (FTIR) spectra of composites are shown in Figure S4, SI section. The characteristic stretch bands of pure PS are observed in 3059.1, 3026.3, 2922.1, and 2846.6 cm^{-1}, resulting from axial deformations of CH$_2$. The absorptions in 1600.9, 1492.7 and 1452.2 cm^{-1} correspond to the C−C elongations of the aromatic ring; 1028.0 cm^{-1} to the C−H curvature in the plane of the phenyl ring and 757.0, 698.2 and 538.1 cm^{-1} are related to C−H deformation of aromatics out-of-plane bending vibration absorption.[82-84] In Figure S4, SI section, it is observed that the variation of the Ag concentration

in relation to PS resulted in different intensities in the absorption of that bands, which can possibly be attributed to the intermolecular interaction between polymer and the surface of the AgNP.[84]

Displacements are observed and all occurred for smaller wavenumber values. Wavenumber displacement from 3082 to 3081 cm^{-1} refers to the aromatic vibrations of CH stretching, while the displacement from 3026 to 3205 cm^{-1} refer to the axial deformations of CH$_2$. In this sense, the greatest displacement was in the CH deformation of aromatics, from 1028 to 1027 cm^{-1} and from 757 to 755 cm^{-1}.[82,83] It is noticeable that the changes occurring in the system are directly related to displacements in stretches of the aromatic ring, indicating that the aromatic ring of the PS is the responsible for most of the interactions between the polymer matrix and the AgNP[84] (Table S1, SI section).

Figure 4 shows the powder XRD patterns of the PS foams and the nanocomposite phases obtained with different amounts of PS. The samples doped with silver ions, PS(5)/AgNP(0.2) and PS(7)/AgNP(0.2) (Figure 4a), presented two distinct diffraction peaks at 2θ = 38.2 and 44.2° corresponding, respectively, to the (111) and (200) crystalline planes of cubic silver (JCPDS 04-0783).[85,86] The peaks show a low relative intensity due to the reduced amount of silver (0.2% by weight, see Experimental
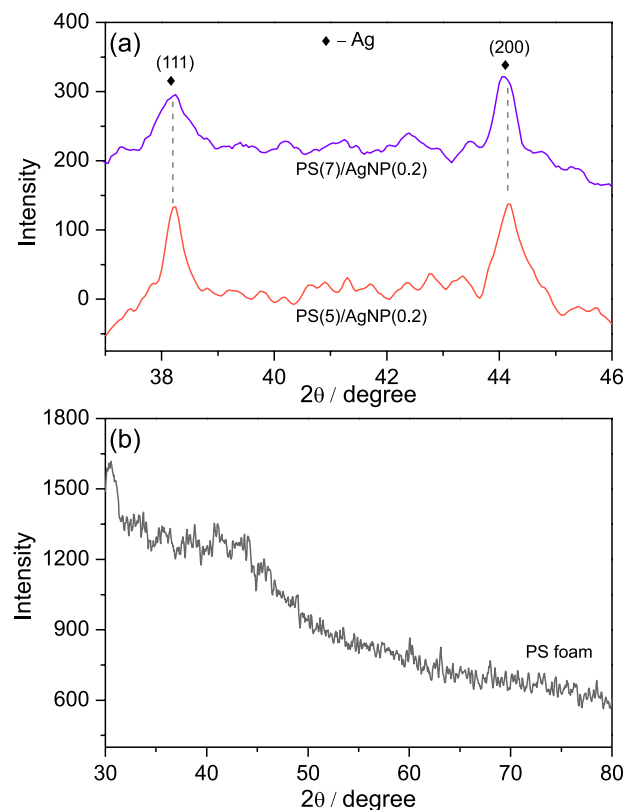
Figure 4. XRD powder pattern of silver doped PS nanocomposite (a) PS(5)/AgNP(0.2) and PS(7)/AgNP(0.2), (b) XRD analysis of PS foam.

section) in PS nanocomposite. As expected, the PS foam sample (Figure 4b) has only the characteristic halo of amorphous materials.[6,83]

The catalyst foam was investigated by LIBS technique for the elemental analysis (Figure 5). The undoped PS sample (Figure 5a) shows the characteristic atomic lines of C (247.8 nm), H (656.4 nm), N (744.2, 746.8, 818.7, 821.6, and 824.3 nm), and O (777.3 nm). The sodium doublet at 589.0 and 589.6 nm was noticed as a contaminant. Additionally, the molecular lines at 358.4, 386.1, 387.1, 415.3, and 415.8 nm can be assigned to CN for Ag-doped and undoped sample. The Ag-doped sample (Figure 5b) shows these lines and the Ag lines at 328.1, 338.2, 520.8, and 546.6 nm, corroborating with the XRD analysis and indicating the presence of Ag impregnated in the foam.
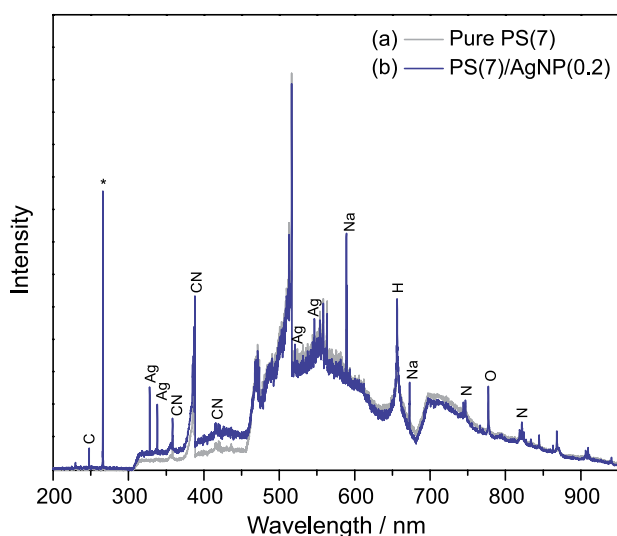
Figure 5. Representative LIBS spectrum of PS samples from 200-950 nm (a) undoped sample PS(7) and (b) PS(7)/AgNP(0.2). The * symbol indicates the 266 nm laser line.

Catalytic tests

The catalytic efficiency of PS/AgNP nanocomposites was investigated in the reduction of PNP to PAP in aqueous medium using NaBH$_4$ as a reducing agent. Borohydride is relatively environmentally friendly because of the low toxicity of borates.[87,88] PNP has a characteristic absorption band at 315 nm (Figure 6a). The color of the PNP solution changes from light yellow to bright yellow after addition of NaBH$_4$, resulting in a spectral shift from 315 to 400 nm, which is caused by the formation of *p*-nitrophenolate ions under alkaline conditions due to hydroxyl group deprotonation[87,89] (Figure 6b). Under alkaline conditions, the decomposition of borohydride is much slower than in acidic medium, favoring its reducing role. During the catalytic reduction reaction, it is observed that there was

a decrease in absorbance, with the appearance of a band at 300 nm, characteristic of PAP (Figure 6a). The reaction kinetics was monitored following the absorbance at 400 nm.

As a control experiment, no significant change was observed after 1 h in the intensity of the band in PNP absorption after the addition of NaBH$_4$ in the absence of PS/AgNP(0.2) (Figure 6c), indicating that the reduction of PNP does not occur without the catalyst. This means that the reduction of PNP in the presence of NaBH$_4$ is thermodynamically favorable, but kinetically unfavorable,[90] due to the high kinetic barrier present between the borohydride and *p*-nitrophenolate anions.[91] Although the reaction is a thermodynamically feasible process involving standard reduction potential (E$_0$) for 4-NP/4-AP = −0.76 V and H$_3$BO$_3$/BH$_4^-$ = −1.33 V *versus* normal hydrogen electrode (NHE), it is kinetically restricted (according to Saha *et al.*,[87] it does not occur even in 2 days' time) in the absence of a catalyst. The kinetic barrier between the mutually repelling negative ions PNP and BH$_4^-$ is very high.[92,93] According to the traditional theory about the catalytic reduction of PNP by metallic nanoparticles, electron transfer takes place from BH$_4^-$ to PNP through adsorption of reactant molecules onto the metallic nanoparticle surface.[93] Metallic nanoparticles relay electrons to complete the redox reaction. The adsorption of reactant ions onto the particle surface contributes to overcoming the kinetic barrier of the reaction.[92] In the presence of PS(5)/AgNP(0.2), an instantaneous decrease in absorption intensity at 400 nm was observed accompanied by the appearance of a smaller band at 300 nm, which indicated the formation of PAP, demonstrating the conversion of PNP to PAP after 45 min (Figure S5, SI section).

Effect of PS concentration

The catalytic efficiency of PS(5)/AgNP and PS(7)/AgNP nanocomposites was investigated in the reduction of PNP to PAP in aqueous medium using NaBH$_4$ as a reducing agent. To evaluate the influence of the PS concentration, the polymer concentration in the PS/AgNP nanocomposite varied, and it was observed that the increase in the PS concentration allowed a greater efficiency in the catalytic reduction, reducing the reaction time of conversion to 30 min, according to Figures 7a and 7b, as opposed to what was predicted when discussing electron microscopy images, as the higher concentration of PS used as support allows for the existence of tighter pores, which makes the NPs have less contact with the PNP dye in the reduction process.[94] This apparent contradiction can be understood considering the Ag/PS ratio for the PS(5)/AgNP(0.2) and PS(7)/AgNP(0.2) systems, which increases with the
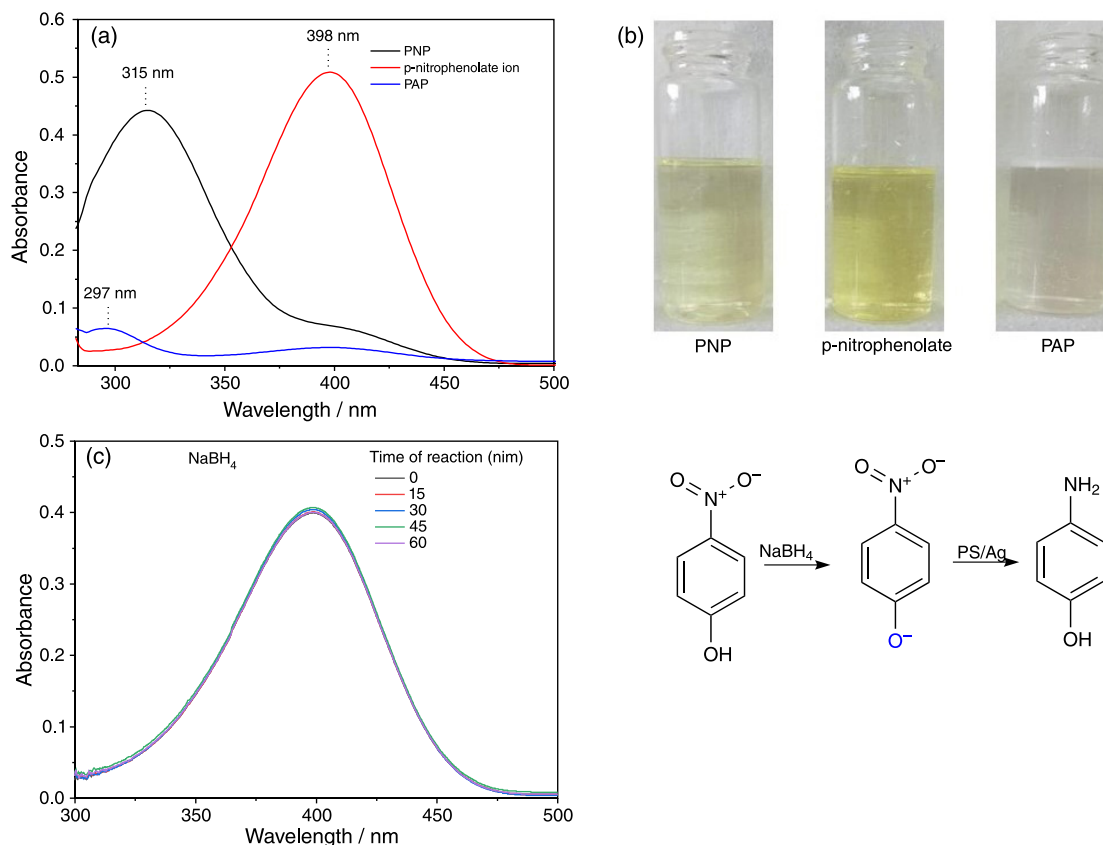
Figure 6. (a) Absorption curves of PNP, *p*-nitrophenolate ion and PAP, (b) PNP, *p*-nitrophenolate ion, and PAP solutions, and (c) catalytic test without PS/AgNP. Parameters: [PNP] = 5×10^{-4}, [NaBH$_4$] = 0.66.

increase in PS, so PS(7)/AgNP(0.2) has a higher absolute amount of Ag than the same mass of PS(5)/AgNP(0.2), leading to greater catalytic activity.

The observed reactions fit well with zero-order kinetics, as reported by Saha *et al.*,[87] Shah *et al.*,[95] and Fedorczyk *et al.*,[96] The increase in catalytic activity is in agreement with the reaction rates achieved by the kinetic constants, which in the presence of PS(5)/AgNP(0.2) (k = 1.16×10^{-2} mol min^{-1}) presented a 35% smaller kinetic constant when compared to PS(7)/AgNP(0.2) (k = 1.77×10^{-2} mol min^{-1}). Furthermore, reduction of PNP to PAP for the tests taking into account a time of 30 min was 73.0% for PS(5)/AgNP(0.2) and 97.7% for PS(7)/AgNP(0.2), in line with the differences in kinetic constants.

Effect of Ag concentration

The concentration of Ag in the PS(5)/AgNP nanocomposite was also investigated, where two different concentrations were studied (0.2 and 0.4%) (Figure S6, SI section). Considering that the reaction was adjusted to zero-order kinetics, samples with 0.4% Ag showed greater catalytic efficiency. For the test using PS(5)/AgNP(0.2)

the velocity constant (k) was 1.16×10^{-2} mol min^{-1} (Table S2, SI section), whereas for PS(5)/AgNP(0.4) k was 1.41×10^{-2} mol min^{-1} and considering the time of 30 min in the process, the reduction percentage was 81.9 and 97% for PS(5)/AgNP(0.2) and PS(5)/AgNP(0.4), respectively. As the concentration of silver nanoparticles increases, the rate of reduction of PNP increases because of its increase in Fermi potential (Table S2, SI section), similarly to the results presented by Narayanan *et al.*[97] Furthermore, increasing the concentration of silver in the reaction medium increases the number of active sites available to catalyze the PNP reduction reaction. This confirms that the increase in the amount of Ag in the system directly influences the reduction process.

Similar results were described by Kastner and Thunemann,[98] where they verified that AgNP coated with poly(acrylic acid), in amounts that varied between 4-13% of Ag, when using a greater amount of catalyst, all PNP had already been reduced at greater velocity. On the other hand, smaller amounts of Ag increased the reaction time. However, this study uses AgNP with sizes of 31 nm, considerably larger than the 5nm AgNP used by Kastner and Thunemann.[98] The use of a larger amount of AgNP was also able to show the efficiency in increasing the reaction
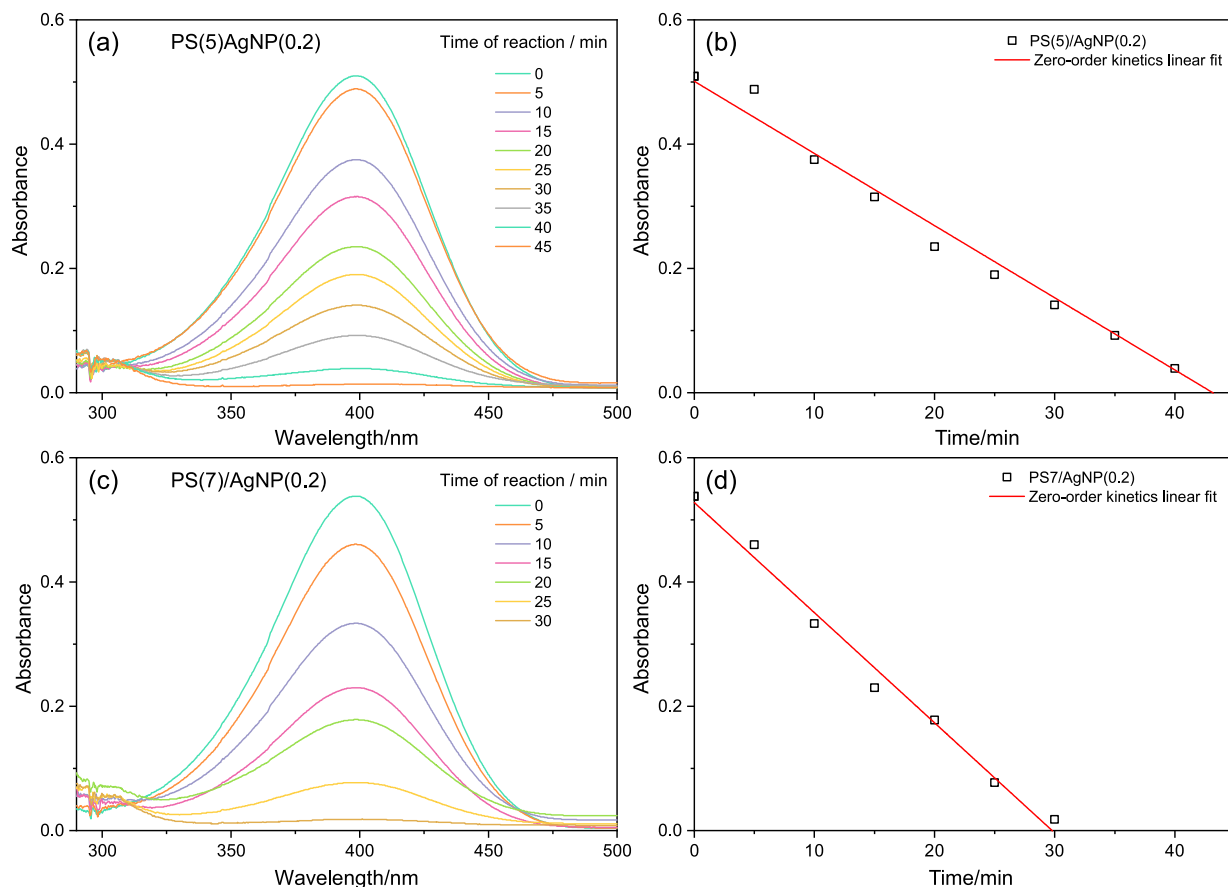
Figure 7. Evaluation of PS concentration (a, c) PS(5)/AgNP(0.2) and PS(7)/Ag(0.2), respectively, (b, d) degradation kinetics for PS(5)/AgNP(0.2) and PS(7)/Ag(0.2), respectively. Parameters: [Ag] = 0.2%; [PNP] = 5 × 10^{-4}; PNP:NaBH$_4$ = 1:1320 (NaBH$_4$:0.66 mol L^{-1}).

rate, resulting in a constant to 1.41 × 10^{-2} mol min^{-1} for PS(5)/AgNP(0.4) (Table S2, SI section). A greater amount of particles simply also corresponds to a greater surface area and availability of active sites.[97]

Effect of the amount of NaBH$_4$

The catalytic reduction of PNP (5 × 10^{-4} mol L^{-1}) using PS(5)/AgNP(0.2) and different amounts of NaBH$_4$ was studied (Figure S7, SI section) and showed that the use of a concentration of NaBH$_4$ equal to 0.50 mol L^{-1} resulted in a slower reaction rate when compared to the test which used a concentration of 0.66 mol L^{-1} (Figure 7a) and 3.3 mol L^{-1} (Figure S7, SI section). In the latter case, the reaction rate increased considerably, when compared to low concentrations of NaBH$_4$, which can be proven through the values of the catalytic rate (Table S3, SI section). Furthermore, it is important to highlight that the concentration of 0.66 mol L^{-1} of NaBH$_4$ is close to the ideal for studies of this nature[87] and therefore it was chosen for the present study (Figure 7a). In the presence of high amounts of NaBH$_4$, the PNP to PAP conversion may not be fully finalized, since a considerable part of the hydrogen

formed from the decomposition of NaBH$_4$ is not directly converted to PNP reduction.[99] Fenger *et al.*[100] discussed that very large amounts of NaBH$_4$ in relation to PNP can compromise the efficiency of the catalytic process and, therefore, the excess of NaBH$_4$ must exist, but be equal to or close to 1000 times in relation to the substrate used.

All tests fit well to zero-order kinetics, this may be the result of the entrapment of the catalyst in a porous support which can cause the concentration of PNP entering the small pores to present a high concentration of PNP at that location and, similarly to NaBH$_4$, can be considered invariant.[95]

Gao *et al.*[101] explains that similar situations presenting zero-order kinetics also occur when the molar ratios of PNP to NaHB$_4$ ([PNP]/[NaHB$_4$]) are smaller, being able to adjust to both zero-order and pseudo-first-order kinetics when the reductant concentration greatly increases in relation to the dye concentration. Some works dealing with the reduction of PNP are listed on the Table 1, and some of these involve the application of supported catalysts that imparts efficiency to the process.

Saha *et al.*[87] used an Ag/CA system as a catalyst in a PNP:NaBH$_4$ molar ratio of 1:1000, similar to the one

Table 1. PNP reduction using different catalytic systems

Catalytic system	PNP / (mol L^{-1})	NaBH$_4$ / (mol L^{-1})	AgNP / %	Reaction order	k	R^2	Reference
Ag/CA	1×10^{-4}	0.1	0.6	zero order	1.04×10^{-5} mol min^{-1}	0.97	87
Ag-SiO$_2$	1×10^{-4}	0.2	5.0	pseudo-first order	0.88 min^{-1}	0.95	102
Ag-Al$_2$O$_3$	1×10^{-4}	0.2	2.0	pseudo-first order	0.35 min^{-1}	0.98	102
PS/AgNP	5×10^{-4}	0.66	0.2	zero order	1.16×10^{-2} mol min^{-1}	0.98	this work

CA: calcium-alginate; PNP: *p*-nitrophenol; AgNP: Ag nanoparticles; k: kinetic constant; R^2: correlation coefficient.

presented in this work. However, although the authors use larger amounts of catalyst in the process, this does not promote a better reaction yield, and results in a kinetic constant value approximately 1000 times smaller in relation to this work, which leads to the conclusion that the material under study showed good catalytic activity, since it showed a higher reaction rate even using a smaller amount of catalyst in concentrated PNP solution.

Influence of the blue light on the plasmon-assisted photocatalytic process

The blue light irradiation in the plasmonic photocatalytic process produces, specifically on the surface of metallic nanoparticles, including AgNP, a greater photon flux and these are able to directly induce reactions of adsorbed reactant molecules, thus increasing the catalytic activity.[103,104]

In the present investigation, the influence of blue light on the photocatalytic reduction of PNP in the presence of PS(5)/AgNP(0.2) and PS(7)/AgNP(0.2) was monitored by UV-Vis spectroscopy (absorption band for monitoring at 400 nm). After addition of PS(5)/AgNP(0.2) or PS(7)/AgNP(0.2) and exposure to blue light, the intensity of this absorption band decreased markedly (Figure S8, SI section). AgNP have energy absorption at maximum wavelength in the emission range promoted in the blue spectral region, collectively exciting the surface plasmon, favoring the catalysis of some reactions such as ethanol oxidation[105] and CO$_2$ reduction.[106] It is important to mention that, to the best of our knowledge, that it is the first time that polystyrene residues are used as a support for AgNP applied in blue light photocatalysis reactions to reduce PNP.

When using PS(5)/AgNP(0.2), it was observed that the photocatalytic reaction showed an increase in the reduction rate, reducing PNP to PAP (98.0%) in just 20 min. This photocatalytic reaction showed a higher velocity constant when compared to the thermocatalytic process in the absence of light, which reached a 53.8% of reduction in 20 min of reaction considering an analysis for total time of 20 min (Figure S8, SI section and Table 2). Figure 7 discussed earlier shows the thermocatalytic reaction for the same catalysts. The rate constants for both reactions are described in Table 2. As observed, without light, the velocity constant for PS(5)/AgNP(0.2) was k = 1.16×10^{-2} mol min^{-1}; on the other hand, the presence of light for the same catalyst significantly increased the efficiency of the system, with k = 2.70×10^{-2} mol min^{-1}. A similar trend was verified when the catalyst used was PS(7)/AgNP(0.2), presenting a higher reaction rate for the photocatalytic test.

The results showed an increase in the rate constant for the photocatalytic reactions. The kinetic rate constant was increased in the same direction for PS(5)/AgNP(0.2)-photocatalytic and PS(7)/AgNP(0.2)-photocatalytic, which gave values of 2.70×10^{-2} and 2.26×10^{-2} mol min^{-1}, respectively (Table 2). Also, the highest rate constant was observed for the nanocomposite with the lowest polymer content PS(5)/AgNP(0.2), this may be related to the coating of active sites on the photocatalyst surface by the high amount of polymer in PS(7)/AgNP(0.2), as well as can be explained by comparing the pore sizes observed in the SEM images, Figure 3. The foams with higher amount of PS may scatter more photons due to smaller pore size, decreasing the amount of light that achieves AgNP catalytic sites.

Table 2. Kinetic constants of photocatalytic and thermocatalytic systems obtained with zero-order kinetic adjustment

Catalytic system	Kinetic constant (k) / (mol min^{-1})	R^2
PS(5)/AgNP(0.2)-thermocatalytic	1.16×10^{-2}	0.98434
PS(5)/AgNP(0.2)-photocatalytic	2.70×10^{-2}	0.98126
PS(7)/AgNP(0.2)-thermocatalytic	1.77×10^{-2}	0.99038
PS(7)/AgNP(0.2)-photocatalytic	2.26×10^{-2}	0.98908

R^2: correlation coefficient.

The catalysts presented here have higher efficiencies when under blue light, since, when carrying out photocatalytic tests using PS(5)/AgNP(0.2), the reaction rate was 2.70×10^{-2} mol min^{-1} with 98% catalytic reduction in just 20 min, compared to the thermocatalytic test showing a decrease to 1.16×10^{-2} mol min^{-1} with 53.8% in the same time interval. A similar result occurred when using PS(7)/AgNP(0.2), showing a decrease in the reaction rate from 2.26×10^{-2} to 1.77×10^{-2} mol min^{-1} with a reduction rate of 96.6 and 85.7% for the photocatalytic and

thermocatalytic ways in 20 min, respectively. One of the advantages of using AgNP as photocatalysts is that they can be activated in the visible and UV range due to the SPR and their inter-band transition properties.[84] Electron excitation from the AgNP sp band to the d band involves the absorption of light in the visible region.[103,107]

In heterogeneous photocatalysis, and specifically in the PNP reduction process, if the incident light does not have enough energy to excite the electron causing it to be promoted from the valence band to the conduction band, they recombine quickly. Therefore, it is important to use radiation that excites the semiconductor at the wavelength at which it absorbs energy, which allows for slower recombination, thus leaving the electrons free on the surface and available to participate in the reduction process,[108] in the case of plasmonic effect-mediated photocatalysis, localized surface plasmons excited on the surface of nanoparticles, for example AgNP, could non-radioactively decay into hot electrons, i.e., holes. The hot electrons could scatter in the excited state of the absorbed molecules and proceed chemical, thus, reactions by lowering the activation energy.[109] In this context, the use of photocatalysis in the PNP reduction process is very favorable and can be one of the good options to be used for such purposes. This can also be verified by means of the reaction rate constant values, which are higher for the photocatalytic test considering the total reduction of PNP.

Conclusions

Silver nanoparticles with diameters of 31 nm were synthesized using the microemulsion method proposed by Hollamby *et al.*,[58] which proved to be quite efficient. The parameters studied in the AgNP synthesis process such as [NaBH$_4$], [AgNO$_3$], [CTAB] and the purification time of the nanoparticles are important parameters since nanoparticles synthesized using parameters smaller than: [NaBH$_4$] = 3.82 mol L^{-1}, [AgNO$_3$] = 0.382 mol L^{-1}, [CTAB] = 0.27 mol L^{-1}, and purification time = 1440 min did not show the smallest particle size. The UV-Vis technique showed that the intensity of the absorption peak increased with increasing concentration of reducing agent, resulting in narrower peaks and smaller particles as the concentrations of the surfactant Ag salt. When obtaining the pure and impregnated foams, the synthesis efficiency resulted from the TIPS. Taking this into account, the presence of AgNP on the surface of the support PS was confirmed by XRD with the appearance of characteristic peaks of Ag in the polymeric support, as well as by interactions occurring in the FTIR resulting from shifts in wavenumbers and variations in intensity. In addition,

SEM showed that the pore distribution of samples with 5% PS showed more open pores facilitating the catalytic process. The samples tested in PNP reduction proved to be very promising, revealing a great efficiency in the reduction process in a PNP:NaBH$_4$ ratio of 1:1320. The catalyst with a small amount equal to 0.2% by mass, using PS(5)/AgNP(0.2) and considering a reduction time of 20 min, reached 98% reduction for photocatalytic tests and 53.8% for thermocatalytic tests. The PS(5)/AgNP(0.2) sample had an excellent efficiency, especially when using a blue color emission light, which presented k = 2.70 × 10^{-2} mol min^{-1}, resulting in a higher reaction rate, when compared to k = 1.16 × 10^{-2} mol min^{-1} for sample without the use of light. The PS(7)/AgNP(0.2) sample was also more efficient for photocatalytic tests, which reveals that small amounts of catalyst in polymeric matrices are promising, especially when emitting lights which increase the reaction rate. Furthermore, larger amounts of catalyst can increase the rate of reduction and, depending on the concentration of the support, it can influence the catalytic process.

Supplementary Information

Supplementary information (Figures S1-S8 and Tables S1-S3) is available free of charge at http://jbcs.sbq.org.br as a PDF file.

Acknowledgments

Author Contributions

W.T.A.S. was responsible for methodology, investigation, writing-original draft; G.C.A. for investigation, formal analysis, writing-original draft, writing-review and editing; R.A.J. for methodology, formal analysis, writing-original draft, writing-review and editing; R.J.B.M. for formal analysis, writing-review and editing; L.F.R.F. for writing-review and editing; Y.P.M.R. and A.G. for methodology, investigation, writing-review and editing; R.S. for methodology, investigation, methodology, formal analysis, writing-review and editing; R.J.O. for conceptualization, formal analysis, writing-review and editing, supervision, project administration, funding acquisition. All authors have read and agreed to the published version of the manuscript.

References

1. Ouyang, B.; Xu, W.; Zhang, W.; Guang, C.; Mu, W.; *J. Environ. Chem. Eng.* **2022**, *10*, 108211. [Crossref]

2. Gao, Y.; Liu, Y.; *J. Environ. Chem. Eng.* **2022**, *10*, 108197. [Crossref]

3. Fallah, Z.; Zare, E. N.; Ghomi, M.; Ahmadijokani, F.; Amini, M.; Tajbakhsh, M.; Arjmand, M.; Sharma, G.; Ali, H.; Ahmad, A.; Makvandi, P.; Lichtfouse, E.; Sillanpää, M.; Varma, R. S.; *Chemosphere* **2021**, *275*, 130055. [Crossref]

4. Bergua, F.; Castro, M.; Muñoz-Embid, J.; Lafuente, C.; Artal, M.; *Chem. Eng. J.* **2021**, *411*, 128472. [Crossref]

5. Kurade, M. B.; Ha, Y.-H.; Xiong, J.-Q.; Govindwar, S. P.; Jang, M.; Jeon, B.-H.; *Chem. Eng. J.* **2021**, *415*, 129040. [Crossref]

6. de Assis, G. C.; Skovroinski, E.; Leite, V. D.; Rodrigues, M. O.; Galembeck, A.; Alves, M. C. F.; Eastoe, J.; de Oliveira, R. J.; *ACS Appl. Mater. Interfaces* **2018**, *10*, 8077. [Crossref]

7. Alula, M. T.; Aragaw, B. A.; Modukanele, S. T.; Yang, J.; *Inorg. Chem. Commun.* **2021**, *127*, 108504. [Crossref]

8. Tchieno, F. M. M.; Tonle, I. K.; *Rev. Anal. Chem.* **2018**, *27*. [Crossref]

9. Wang, P.; Tang, L.; Wei, X.; Zeng, G.; Zhou, Y.; Deng, Y.; Wang, J.; Xie, Z.; Fang, W.; *Appl. Surf. Sci.* **2017**, *392*, 391. [Crossref]

10. Dias, R.; Oliveira, H.; Fernandes, I.; Simal-Gandara, J.; Perez-Gregorio, R.; *Crit. Rev. Food Sci. Nutr.* **2021**, *61*, 1130. [Crossref]

11. Anku, W. W.; Mamo, M. A.; Govender, P. P. In *Phenolic Compounds*; Soto-Hernandez, M.; Palma-Tenango, M.; Garcia-Mateos, M., eds.; InTech, 2017. [Crossref]

12. Boruah, P. K.; Sharma, B.; Karbhal, I.; Shelke, M. V.; Das, M. R.; *J. Hazard. Mater.* **2017**, *325*, 90. [Crossref]

13. Falcone, G.; Giuffrè, O.; Sammartano, S.; *J. Mol. Liq.* **2011**, *159*, 146. [Crossref]

14. Naaz, F.; Shamsi, A.; Jain, S. K.; Kalam, A.; Ahmad, T.; *Mater. Today: Proc.* **2020**, *36*, 708. [Crossref]

15. Pradhan, N.; Pal, A.; Pal, T.; *Colloids Surf., A* **2002**, *196*, 247. [Crossref]

16. Shimoga, G.; Palem, R. R.; Lee, S.-H.; Kim, S.-Y.; *Metals (Basel)* **2020**, *10*, 1661. [Crossref]

17. Younis, S. A.; Amdeha, E.; El-Salamony, R. A.; *J. Environ. Chem. Eng.* **2021**, *9*, 104619. [Crossref]

18. Skiba, M.; Vorobyova, V.; Pivovarov, A.; Trus, I.; *Pigm. Resin Technol.* **2020**, *49*, 449. [Crossref]

19. Yang, J.; Shen, X.; Ji, Z.; Zhou, H.; Zhu, G.; Chen, K.; *Ceram. Int.* **2015**, *41*, 4056. [Crossref]

20. Nguyen, T. B.; Huang, C. P.; Doong, R.; *Appl. Catal. B* **2019**, *240*, 337. [Crossref]

21. Roy, D.; Neogi, S.; De, S.; *J. Environ. Chem. Eng.* **2021**, *9*, 106677. [Crossref]

22. Wu, H.; Wu, Z.; Liu, B.; Zhao, X.; *ACS Omega* **2020**, *21*, 11998. [Crossref]

23. Wu, J.; Wang, J.; Wang, T.; Sun, L.; Du, Y.; Li, Y.; Li, H.; *Appl. Surf. Sci.* **2019**, *466*, 342. [Crossref]

24. Rodrigues, T. S.; da Silva, A. G. M.; Camargo, P. H. C.; *J. Mater. Chem. A* **2019**, *7*, 5857. [Crossref]

25. Sagitha, P.; Sarada, K.; Muraleedharan, K.; *Trans. Nonferrous Met. Soc. China* **2016**, *26*, 2693. [Crossref]

26. Chishti, A. N.; Ni, L.; Guo, F.; Lin, X.; Liu, Y.; Wu, H.; Chen, M.; Diao, G. W.; *J. Environ. Chem. Eng.* **2021**, *9*, 104948. [Crossref]

27. Benamara, M.; Gómez, E.; Dhahri, R.; Serrà, A.; *Toxins* **2021**, *13*, 66. [Crossref]

28. Nakamura, S.; Sato, M.; Sato, Y.; Ando, N.; Takayama, T.; Fujita, M.; Ishihara, M.; *Int. J. Mol. Sci.* **2019**, *20*, 3620. [Crossref]

29. dos Santos Jr., V. E.; Targino, A. G. R.; Flores, M. A. P.; Rodríguez-Díaz, J. M.; Teixeira, J. A.; Heimer, M. V.; Pessoa, H. L. F.; Galembeck, A.; Rosenblatt, A.; *Res. Chem. Intermed.* **2017**, *43*, 5889. [Crossref]

30. Cortés, E.; Besteiro, L.V.; Alabastri, A.; Baldi, A.; Tagliabue, G.; Demetriadou, A.; Narang, P.; *ACS Nano* **2020**, *14*, 16202. [Crossref]

31. Schatz, G. C.; *Chem. Res.* **1984**, *10*, 370. [Crossref]

32. de Souza, M. L.; dos Santos, D. P.; Corio, P.; *RSC Adv.* **2018**, *8*, 28753. [Crossref]

33. Horlyck, J.; Lovell, E.; Scott, J.; *Catal. Lett.* **2021**, *152*, 619. [Crossref]

34. Furube, A.; Hashimoto, S.; *NPG Asia Materials* **2017**, *9*, e454. [Crossref]

35. Ahlawat, M.; Mittal, D.; Rao, V. G.; *Commun. Mater.* **2021**, *2*, 114. [Crossref]

36. Chen, X.; Zheng, Z.; Ke, X.; Jaatinen, E.; Xie, T.; Wang, D.; Guo, C.; Zhao, J.; Zhu, H.; *Green Chem.* **2010**, *12*, 414. [Crossref]

37. Shang, L.; Liang, Y.; Li, M.; Waterhouse, G. I. N.; Tang, P.; Ma, D.; Wu, L.-Z.; Tung, C.-H.; Zhang, T.; *Adv. Funct. Mater.* **2017**, *27*, 1606215. [Crossref]

38. Poupart, R.; Grande, D.; Carbonnier, B.; Le Droumaguet, B.; *Prog. Polym. Sci.* **2019**, *96*, 21. [Crossref]

39. Nasrollahzadeh, M.; Sajjadi, M.; Shokouhimehr, M.; Varma, R. S.; *Coord. Chem. Rev.* **2019**, *397*, 54. [Crossref]

40. Dolatkhah, A.; Jani, P.; Wilson, L. D.; *Langmuir* **2018**, *34*, 10560. [Crossref]

41. Ji, T.; Chen, L.; Mu, L.; Yuan, R.; Knoblauch, M.; Bao, F. S.; Zhu, J.; *Appl. Catal., B* **2016**, *182*, 306. [Crossref]

42. Khrizanforov, M. N.; Fedorenko, S. V.; Mustafina, A. R.; Kholin, K. V.; Nizameev, I. R.; Strekalova, S. O.; Grinenko, V. V.; Gryaznova, T. V.; Zairov, R. R.; Mazzaro, R.; Morandi, V.; Vomiero, A.; Budnikova, Y. H.; *Dalton Trans.* **2018**, *47*, 9608. [Crossref]

43. Xiao, G.; Zhao, Y.; Li, L.; Pratt, J. O.; Su, H.; Tan, T.; *Nanotechnology* **2018**, *29*, 155601. [Crossref]

44. Tan, L.; Tan, B.; *Chem. Eng. J.* **2020**, *390*, 124485. [Crossref]

45. Shah, J.; Jan, M. R.; Adnan; Zada, M.; *Process Saf. Environ. Prot.* **2015**, *96*, 149. [Crossref]

46. Van Deelen, T. W.; Hernández Mejía, C.; de Jong, K. P.; *Nat. Catal.* **2019**, *2*, 955. [Crossref]

47. Turner, A.; *Chemosphere* **2021**, *263*, 128087. [Crossref]

48. Li, Y.; Hu, Y.; Ye, S.; Wu, Y.; Yang, C.; Wang, L.; *New J. Chem.* **2016**, *40*, 10398. [Crossref]

49. Kaboudin, B.; Khanmohammadi, H.; Kazemi, F.; *Appl. Surf. Sci.* **2017**, *425*, 400. [Crossref]

50. Clot-Almenara, L.; Rodríguez-Escrich, C.; Osorio-Planes, L.; Pericàs, M. A.; *ACS Catal.* **2016**, *6*, 7647. [Crossref]

51. Aubert, J. H.; Clough, R. L.; *Polymer* **1985**, *26*, 2047. [Crossref]

52. Steytler, D. C.; Robinson, B. H.; Eastoe, J.; Ibel, K.; Dore, J. C.; MacDonald, I.; *Langmuir* **1993**, *9*, 903. [Crossref]

53. Nogueira, J. C. F.; Paliashvili, K.; Bradford, A.; Di Maggio, F.; Richards, D. A.; Day, R. M.; Chudasama, V.; *Org. Biomol. Chem.* **2020**, *18*, 2215. [Crossref]

54. Sandoval, C.; Molina, G.; Jentzsch, P. V.; Pérez, J.; Muñoz, F.; *J. Adv. Oxid. Technol.* **2017**, *20*, 20170006. [Crossref]

55. Valadez-Renteria, E.; Barrera-Rendon, E.; Oliva, J.; Rodriguez-Gonzalez, V.; *Sep. Purif. Technol.* **2021**, *270*, 118821. [Crossref]

56. Sandhu, S.; Krishnan, S.; Karim, A. V.; Shriwastav, A.; *J. Environ. Chem. Eng.* **2020**, *8*, 104471. [Crossref]

57. Rolison, D. R.; *Science* **2003**, *299*, 1698. [Crossref]

58. Hollamby, M. J.; Eastoe, J.; Chemelli, A.; Glatter, O.; Rogers, O.; Heenan, R. K.; Grillo, I.; *Langmuir* **2010**, *26*, 6989. [Crossref]

59. Malik, M. A.; Wani, M. Y.; Hashim, M. A.; *Arabian J. Chem.* **2012**, *5*, 397. [Crossref]

60. Rasband, W. S.; *ImageJ*, version 1.53e; U. S. National Institutes of Health, Bethesda, Maryland, USA, 2020.

61. *NIST Standard Reference Database 78*, version 5.10; NIST, Gaithersburg, USA, 2021. [Crossref]

62. Qian, L.; Zhang, H.; *J. Chem. Technol. Biotechnol.* **2011**, *86*, 172. [Crossref]

63. Mulfinger, L.; Solomon, S. D.; Bahadory, M.; Jeyarajasingam, A. V.; Rutkowsky, S. A.; Boritz, C.; *J. Chem. Educ.* **2007**, *84*, 322. [Crossref]

64. Wang, X.; Cao, Y.; *J. Ind. Eng. Chem.* **2020**, *82*, 324. [Crossref]

65. Thammawithan, S.; Siritongsuk, P.; Nasompag, S.; Daduang, S.; Klaynongsruang, S.; Prapasarakul, N.; Patramanon, R.; *Vet. Sci.* **2021**, *8*, 177. [Crossref]

66. Mie, G.; *Ann. Phys.* **1908**, *330*, 377. [Crossref]

67. Ribeiro, M. S.; de Melo, L. S. A.; Farooq, S.; Baptista, A.; Kato, I. T.; Núñez, S. C.; de Araujo, R. E.; *Photodiagn. Photodyn. Ther*. **2018**, *22*, 191. [Crossref]

68. Li, X.; Shen, J.; Du, A.; Zhang, Z.; Gao, G.; Yang, H.; Wu, J.; *Colloids Surf., A* **2012**, *400*, 73. [Crossref]

69. MiePlot software, www.philiplaven.com/mieplot.htm, accessed in March 2023.

70. Rakib-Uz-Zaman, S. M.; Hoque Apu, E.; Muntasir, M. N.; Mowna, S. A.; Khanom, M. G.; Jahan, S. S.; Akter, N.; Khan, M. A. R.; Shuborna, N. S.; Shams, S. M.; Khan, K.; *Challenges* **2022**, *13*, 18. [Crossref]

71. Anandalakshmi, K.; Venugobal, J.; Ramasamy, V.; *Appl. Nanosci.* **2016**, *6*, 399. [Crossref]

72. Zille, A.; Fernandes, M. M.; Francesko, A.; Tzanov, T.; Fernandes, M.; Oliveira, F. R.; Almeida, L.; Amorim, T.; Carneiro, N.; Esteves, M. F.; Souto, A. P.; *ACS Appl. Mater. Interfaces* **2015**, *7*, 13731. [Crossref]

73. Husein, M. M.; Rodil, E.; Vera, J. H.; *J. Nanopart. Res.* **2007**, *9*, 787. [Crossref]

74. Husein, M. M.; Rodil, E.; Vera, J. H.; *Langmuir* **2003**, *19*, 8467. [Crossref]

75. Husein, M. M.; Rodil, E.; Vera, J. H.; *J. Colloid Interface Sci.* **2004**, *273*, 426. [Crossref]

76. Zhang, W.; Qiao, X.; Chen, J.; *Chem. Phys.* **2008**, *109*, 411. [Crossref]

77. Piella, J.; Bastús, N. G.; Puntes, V.; *Z. Phys. Chem.* **2017**, *231*, 1. [Crossref]

78. Tomaszewska, E.; Soliwoda, K.; Kadziola, K.; Tkacz-Szczesna, B.; Celichowski, G.; Cichomski, M.; Cichomski, W.; Szmaja, J.; Grobelny, J.; *J. Nanomater.* **2013**, ID 313081. [Crossref]

79. Oliveira, J. P.; Prado, A. R.; Keijok, W. J.; Ribeiro, M. R. N.; Pontes, M. J.; Nogueira, B. V.; Guimarães, M. C. C.; *Arabian J. Chem.* **2020**, *13*, 216. [Crossref]

80. Gu, S.; Mogi, T.; Konno, M.; *Colloids Surf., A* **1999**, *153*, 209. [Crossref]

81. Lundqvist, M.; Stigler, J.; Elia, G.; Lynch, I.; Cedervall, T.; Dawson, K.; *Proc. Natl. Acad. Sci. U.S.A.* **2008**, *105*, 14265. [Crossref]

82. Fang, J.; Xuan, Y.; Li, Q.; *Sci. China Technol. Sci*. **2010**, *53*, 3088. [Crossref]

83. Wang, D.; An, J.; Luo, Q.; Li, X.; Li, M.; *J. Appl. Polym. Sci.* **2008**, *110*, 3038. [Crossref]

84. Ismail, R. A.; Almashhadani, N. J.; Sadik, R. H.; *Appl. Nanosci.* **2017**, *7*, 109. [Crossref]

85. Yougen, H.; Tao, Z.; Pengli, Z.; Rong, S.; *Colloid Polym Sci.* **2012**, *290*, 401. [Crossref]

86. Conte, P.; Carotenuto, G.; Piccolo, A.; Perlo, P.; Nicolais, L.; *J. Mater. Chem.* **2007**, *17*, 201. [Crossref]

87. Saha, S.; Pal, A.; Kundu, S.; Basu, S.; Pal, T.; *Langmuir* **2010**, *26*, 2885. [Crossref]

88. Hashimi, A. S.; Nohan, M. A. N. M.; Chin, S. X.; Zakaria, S.; Chia, C. H.; *Nanomaterials* **2019**, *9*, 936. [Crossref]

89. Rezaei, F.; Dinari, M.; *Colloids Surf., A* **2021**, *618*, 126441. [Crossref]

90. Marimuthu, M.; Li, H.; Chen, Q.; *J. Mol. Liq.* **2021**, *333*, 115963. [Crossref]

91. Albukhari, S. M.; Ismail, M.; Akhtar, K.; Danish, E. Y.; *Colloids Surf., A* **2019**, *577*, 548. [Crossref]

92. Li, M.; Chen, G.; *Nanoscale* **2013**, *5*, 11919. [Crossref]

93. Huang, J.; Vongehr, S.; Tang, S.; Lu, H.; Meng, X.; *J. Phys. Chem. C* **2010**, *114*, 15005. [Crossref]

94. Ji, X.; Griesing, F.; Yan, R.; Sun, B.; Pauer, W.; Zhu, M.; Sun, Y.; Moritz, H. U.; *RSC Adv.* **2017**, *7*, 50176. [Crossref]

95. Shah, M. T.; Balouch, A.; Sirajuddin; Pathan, A. A.; Abdullah; Mahar, A. M.; Sabir, S.; Khattak, R.; Umar, A. A.; *Microsyst. Technol.* **2017**, *23*, 5745. [Crossref]

96. Fedorczyk, A.; Ratajczak, J.; Kuzmych, O.; Skompska, M.; *J. Solid State Electrochem.* **2015**, *19*, 2849. [Crossref]

97. Narayanan, K. B.; Park, H. H.; Sakthivel, N.; *Spectrochim. Acta, Part A* **2013**, *16*, 485. [Crossref]

98. Kastner, C.; Thünemann, A. F.; *Langmuir* **2016**, *32*, 7383. [Crossref]

99. Goepel, M.; Al-Naji, M.; With, P.; Wagner, G.; Oeckler, O.; Enke, D.; Gläser, R.; *Chem. Eng. Technol.* **2014**, *37*, 551. [Crossref]

100. Fenger, R.; Fertitta, E.; Kirmse, H.; Thünemann, A. F.; Rademann, K.; *Phys. Chem. Chem. Phys.* **2012**, *14*, 9343. [Crossref]

101. Gao, Y.; Zhao, S.; Zhang, G.; Deng, L.; Li, J.; Sun, R.; Li, L.; Wong, C.-P.; *J. Mater. Sci.* **2015**, *50*, 3399. [Crossref]

102. Feng, J.; Fan, D.; Wang, O.; Ma, L.; Wei, W.; Xie, J.; Zhu, J.; *Colloids Surf., A* **2017**, *520*, 743. [Crossref]

103. Kim, Y.; Smith, J. G.; Jain, P. K.; *Nat. Chem.* **2018**, *10*, 763. [Crossref]

104. Sarina, S.; Waclawik, E. R.; Zhu, H.; *Green Chem.* **2013**, *15*, 1814. [Crossref]

105. Tan, T. H.; Scott, J.; Ng, Y. H.; Taylor, R. A.; Aguey-Zinsou, K. F.; Amal, R.; *ACS Catal.* **2016**, *6*, 1870. [Crossref]

106. Zhang, H.; Itoi, T.; Konishi, T.; Izumi, Y.; *J. Am. Chem. Soc.* **2019**, *141*, 6292. [Crossref]

107. Rani, P.; Kumar, V.; Singh, P. P.; Matharu, A. S.; Zhang, W.; Kim, K. H.; Singh, J.; Rawat, M.; *Environ. Int.* **2020**, *143*, 105924. [Crossref]

108. Hernández-Gordillo, A.; Acevedo-Peña, P.; Bizarro, M.; Rodil, S. E.; Gómez, R.; *J. Mater. Sci.: Mater. Electron.* **2018**, *29*, 7345. [Crossref]

109. Zhang, Z.; Xu, P.; Yang, X.; Liang, W.; Sun, M.; *J. Photochem. Photobiol., C* **2016**, *27*, 100. [Crossref]